

Barut-Girardello coherent states in graphene under uniform uniaxial strain

Y Concha-Sánchez^{*1}, E Díaz-Bautista^{†2}, and A Raya^{‡3}

¹Facultad de Ingeniería Civil, Universidad Michoacana de San Nicolás de Hidalgo, Edificio C, Ciudad Universitaria. Francisco J. Mújica s/n. Col. Felicitas del Río. 58030, Morelia, Michoacán, México

²Physics Department, Cinvestav, P.O. Box. 14-740, 07000 Mexico City, Mexico

³Instituto de Física y Matemáticas, Universidad Michoacana de San Nicolás de Hidalgo, Edificio C-3, Ciudad Universitaria. Francisco J. Mújica s/n. Col. Felicitas del Río. 58040 Morelia, Michoacán, México

Abstract

We construct the Barut-Girardello coherent states for charge carriers in graphene placed in a constant homogeneous magnetic field which is orthogonal to the graphene sample. We consider the situation in which the membrane is deformed uniformly and uniaxially, avoiding the generation of pseudomagnetic fields. For that purpose, we solve the Dirac-Weyl equation with an anisotropic Fermi velocity and identify the appropriate arising and lowering operators. Working in a Landau-like gauge, we explicitly construct nonlinear coherent states as eigenstates of a generalized annihilation operator with complex eigenvalues which depends on an arbitrary function f of the number operator. In order to describe the effects of strain on these states, we obtain the Heisenberg uncertainty relation, the probability density and mean energy value for three different functions f . In general, when the deformation is along the x -axis of the membrane, the probability density obtained for the nonlinear coherent states is smaller than when the deformation is along the orthogonal direction.

1 Introduction

The physical system of a charged particle interacting with a uniform magnetic field has been considered in several works due to its important technological implications. Fock solved the non-relativistic quantum mechanical problem for the first time by defining the magnetic field in the so-called symmetric gauge [1], but Landau addressed the same physical situation by

^{*}yconcha@umich.mx

[†]ediaz@fis.cinvestav.mx

[‡]raya@ifm.umich.mx

choosing a gauge –nowadays known as Landau gauge– that reduces the initial Schrödinger equation to the one-dimensional quantum harmonic oscillator problem [2]. Although trivial at first glance, this fact allows to connect with a well-known system that can be solved algebraically by defining a set of first order differential operators a and a^\dagger , that together with the identity operator are generators of the Heisenberg-Weyl (HW) algebra. Furthermore, for the quantum harmonic oscillator the coherent states describe in semi-classical situations such a system. In fact, Schrödinger [3] proposed the coherent states (CS) as the most classical states describing the motion of a particle in a quadratic potential, they have become a canonical subject in quantum mechanics literature. Moreover, the construction of coherent states has been generalized to other systems through different definitions, e.g., as eigenstates of the annihilation operator of the system (Barut-Girardello CS) [4], or as states obtained by acting the displacement operator on the fundamental state (Gilmore-Perelomov CS) [5–8].

The algebra associated to the arising and lowering operators a^\dagger, a of the harmonic oscillator can be generalized to an f -deformed algebra, which is obtained by replacing them by deformed creation and annihilation operators defined as [9]

$$\mathcal{A} = af(N) = f(N+1)a, \quad \mathcal{A}^\dagger = f(N)a^\dagger = a^\dagger f(N+1), \quad N = a^\dagger a, \quad (1)$$

where f is a well-behaved real function of the standard number operator N , with the corresponding commutators

$$[N, \mathcal{A}] = -\mathcal{A}, \quad [N, \mathcal{A}^\dagger] = \mathcal{A}^\dagger, \quad [\mathcal{A}, \mathcal{A}^\dagger] = (N+1)f^2(N+1) - Nf^2(N). \quad (2)$$

Thus, nonlinear coherent states (NLCS) have been introduced as eigenstates of the deformed annihilation operator $\mathcal{A}|\alpha\rangle_f = \alpha|\alpha\rangle_f$ [9, 10]. In general, such states exhibit nonclassical properties, e.g., squeezing and antibunching [11]. They are also connected with oscillators whose frequency depends on the energy [9, 10, 12], some of them can be obtained physically as stationary states of the center-of-mass motion of a trapped ion [11] or to model the vibrations of polyatomic molecules [13, 14]. It can be concluded that the coherent states construction for a quantum mechanical system is a desirable thing to do.

On the other hand, graphene is a material that consists of a one-atom thick layer of carbon atoms tightly packed in a honeycomb array, with outstanding properties for technological applications and fundamental physics development [15–18]. Its characteristic feature is that at low-energy, also known as the continuum limit, the behavior of its charge carriers is quite similar as for ultra-relativistic fermions, while its dispersion relation is linear. As a consequence, these quasiparticles are described by a Dirac-like equation, instead of the ordinary Schrödinger equation with a typical parabolic dispersion relation.

Recently, an increasing interest to exploit strain for controlling other physical properties of the layer, for example, its stiffness and strength, has arisen due to the outstanding mechanical properties of monolayer graphene. Among the new research subjects worth to be mentioned, straintronics [19] has studied the mechanical deformations of graphene layers to modify its electric properties [20]. Some experimental results about the response of graphene under tensile and compressive strain had been discussed previously [21]. Theoretically, although these mechanical deformations displace and deform the Dirac cones to an elliptic cross-section and induce

a tensor character to the Fermi velocity in graphene, in the low-energy regime the dispersion relation is modified from the ideal case, but the equations of motion are still tractable [20]. In this sense, uniform strain deserves special attention, since it is the limiting case of any general deformation, is solvable and leads to an anisotropic Fermi velocity, but it does not produce any pseudo-magnetic field whatsoever [22, 23]. Due to its theoretical simplicity, uniform strain is useful for describing the effects induced in the dynamics of graphene electrons. Thus, our goal here is to generalize the results in [24] by considering uniform uniaxial strain in the graphene layer and construct the corresponding NLCS.

For that purpose, we have organized this article as follows. In sect. 2 the Dirac-Weyl equation under uniform uniaxial strain is solved in a Landau-like gauge. The corresponding energy spectrum and eigenstates are obtained as functions of the parameters a and b that characterize the uniform uniaxial strain. In sect. 3 a generalized annihilation operator associated to the system is presented and the NLCS are introduced as eigenstates of such a matrix operator. These quantum states are characterized through their probability density, the Heisenberg uncertainty relation and the mean energy value. In sect. 4 we discuss our achievements and present our conclusions.

2 Dirac-Weyl equation under strain

We start from the Dirac-Weyl equation under uniform uniaxial strain [23],

$$H_D \Psi(x, y) = v_F (a \sigma_x \pi_x + b \sigma_y \pi_y) \Psi(x, y) = E \Psi(x, y), \quad (3)$$

where a, b are positive real numbers. This is a simple way to promote the Fermi velocity to a tensor and still avoid the generation of pseudomagnetic fields. Here, $\pi_{x,y} = p_{x,y} + eA_{x,y}/c$, with \vec{p} denoting the canonical momentum and \vec{A} the vector potential which defines a magnetic field aligned perpendicularly to the graphene surface. In a Landau-like gauge,

$$\vec{A}(x, y) = A_y(x) \hat{j}, \quad \vec{B} = \nabla \times \vec{A} = B(x) \hat{k}, \quad (4)$$

such that we can write

$$\Psi(x, y) = \exp(iky) \begin{pmatrix} \psi^+(x) \\ \psi^-(x) \end{pmatrix}. \quad (5)$$

Substituting (5) into (3), two coupled equations arise, namely:

$$\left[ap_x + ib \left(k\hbar + \frac{e}{c} A_y(x) \right) \right] \psi^+(x) = \frac{E}{v_F} \psi^-(x), \quad (6a)$$

$$\left[ap_x - ib \left(k\hbar + \frac{e}{c} A_y(x) \right) \right] \psi^-(x) = \frac{E}{v_F} \psi^+(x). \quad (6b)$$

These equations are decoupled to obtain

$$\left[-\frac{d^2}{dx^2} + V_\zeta^+(x) \right] \psi^+(x) = \epsilon_a^{+2} \psi^+(x), \quad (7a)$$

$$\left[-\frac{d^2}{dx^2} + V_\zeta^-(x) \right] \psi^-(x) = \epsilon_a^{-2} \psi^-(x), \quad (7b)$$

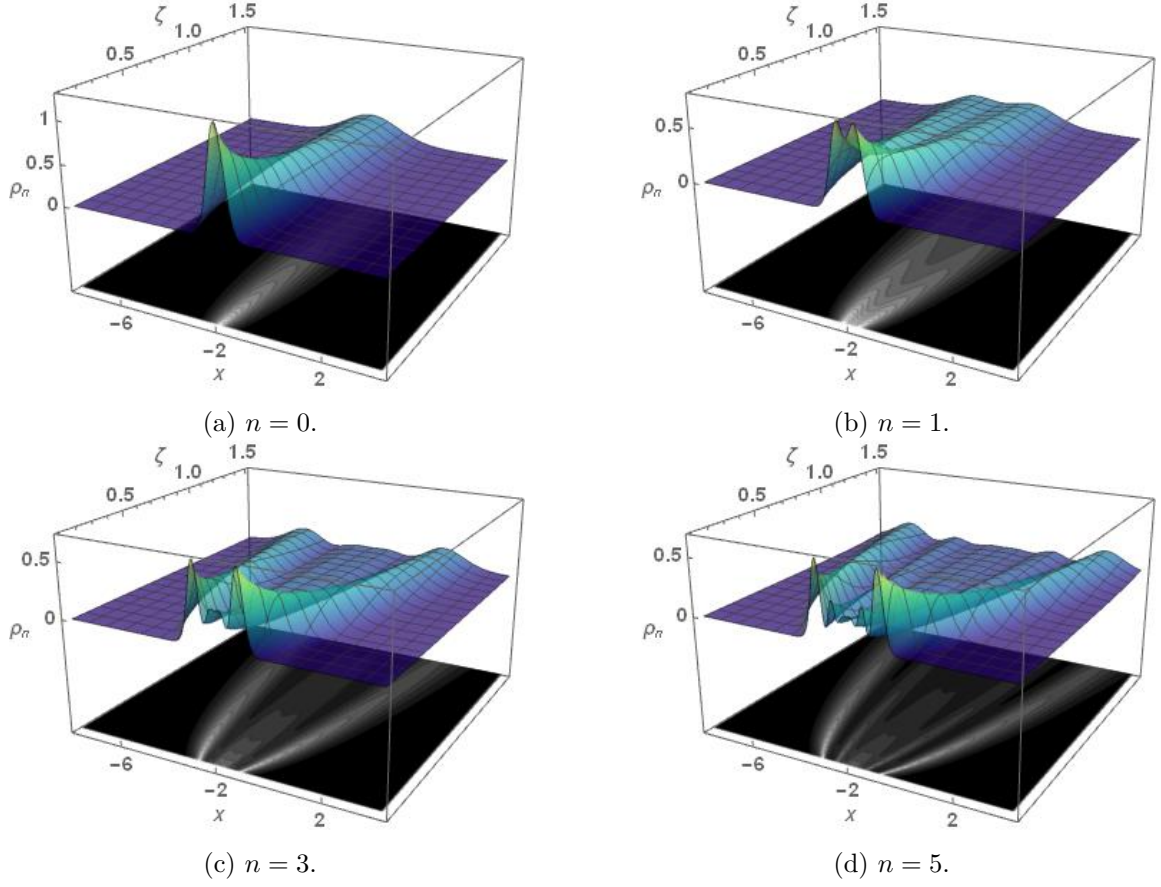


Figure 1: Probability density $\rho_n(x)$ for the pseudo-spinor states $\Psi_n(x, y)$ in Eq. (15) as function of the parameter ζ for different values of n . In all the cases $B_0 = 1/2$, $k = \omega = 1$ and $\zeta \in [1/10, 3/2]$.

where $\epsilon_a^\pm = E/a v_F \hbar$ and

$$V_\zeta^\pm(x) = \left(\frac{k}{\zeta} + \frac{eA_y(x)}{c\hbar\zeta} \right)^2 \pm \frac{e}{c\hbar\zeta} \frac{dA_y(x)}{dx}, \quad \zeta = \frac{a}{b}. \quad (8)$$

In order to describe a uniform magnetic field, we take

$$\vec{A} = B_0 x \hat{j}, \quad \vec{B} = B_0 \hat{k}. \quad (9)$$

Thus, by defining the frequency ω_ζ as

$$\omega_\zeta = \frac{\omega}{\zeta} = \frac{2eB_0}{c\hbar\zeta}, \quad (10)$$

where ω is the cyclotron frequency of electrons in pristine graphene, we get the following Hamiltonians H_ζ^\pm :

$$H_\zeta^\pm = -\frac{d^2}{dx^2} + V_\zeta^\pm(x), \quad V_\zeta^\pm(x) = \frac{\omega_\zeta}{4} \left(x + \frac{2k}{\omega} \right)^2 \pm \frac{1}{2}\omega_\zeta. \quad (11)$$

It follows that:

$$\epsilon_{0,a}^- = 0, \quad \epsilon_{n,a}^- = \epsilon_{n-1,a}^+ = \omega_\zeta n, \quad n = 0, 1, 2, \dots, \quad (12)$$

or, equivalently,

$$E_0^- = 0, \quad E_n^- = E_{n-1}^+ = v_F \hbar \sqrt{ab \omega n}, \quad n = 0, 1, 2, \dots \quad (13)$$

Finally, the corresponding normalized eigenfunctions are given by:

$$\psi_n^\pm(x) = \sqrt{\frac{1}{2^n n!} \left(\frac{\omega_\zeta}{2\pi}\right)^{1/2}} \exp\left[-\frac{\omega_\zeta}{4} \left(x + \frac{2k}{\omega}\right)^2\right] H_n\left[\sqrt{\frac{\omega_\zeta}{2}} \left(x + \frac{2k}{\omega}\right)\right]. \quad (14)$$

Thus, the pseudo-spinor eigenstates are

$$\Psi_n(x, y) = \frac{\exp(iky)}{\sqrt{2^{(1-\delta_{0n})}}} \begin{pmatrix} (1 - \delta_{0n})\psi_{n-1}(x) \\ i\psi_n(x) \end{pmatrix}, \quad n = 0, 1, 2, \dots, \quad (15)$$

where δ_{mn} denotes the Kronecker delta, $\psi_n^- \equiv \psi_n$ and $\psi_n^+ \equiv \psi_{n-1}$.

Figure 1 reveals two interesting facts. First, the probability density $\rho_n(x)$ given by

$$\rho_n(x) = \frac{1}{2^{(1-\delta_{0n})}} [|\psi_n(x)|^2 + (1 - \delta_{0n})|\psi_{n-1}(x)|^2], \quad (16)$$

shows two maximum values in two different positions

$$x_\pm = x_0 \pm \sqrt{\frac{2}{\omega_\zeta}} \eta, \quad (17)$$

where $x_0 = -2k/\omega$ and η is determined by the relation:

$$g_n(\eta) + (1 - \delta_{0n})n g_{n-1}(\eta) = 0, \quad g_n(\eta) = H_n(\eta) [\eta H_n(\eta) - H_{n+1}(\eta)]. \quad (18)$$

The distance between the points x_\pm increases as n and ζ do. In particular, we have that $x_\pm = x_0$ for $n = 0$. Second, for given n , in the limit $\zeta \rightarrow 0$, the function $\rho_n(x)$ takes larger values at the points x_\pm , while in the limit $\zeta \rightarrow \infty$, $\rho_n(x)$ takes values close to zero. In other words, if $b \gg a$ the probability to find the electron around the points x_\pm increases while the distance respect to x_0 decreases. If $a \gg b$, we have the opposite situation.

2.1 Algebraic structure

Let us define the following dimensionless differential operators

$$\theta^\pm = \frac{1}{\sqrt{2}} \left(\mp \frac{d}{d\xi} + \xi \right), \quad \theta^+ = (\theta^-)^\dagger, \quad \xi = \sqrt{\frac{\omega_\zeta}{2}} \left(x + \frac{2k}{\omega} \right), \quad (19)$$

that satisfy the commutation relation

$$[\theta^-, \theta^+] = 1. \quad (20)$$

This relation implies that the set of operators $\{\theta^+, \theta^-, 1\}$ generate a HW algebra.

Now, the action of the operators θ^\pm on the eigenfunctions ψ_n is:

$$\theta^- \psi_n = \sqrt{n} \psi_{n-1}, \quad \theta^+ \psi_n = \sqrt{n+1} \psi_{n+1}, \quad (21)$$

so that θ^- (θ^+) is the annihilation (creation) operator.

In terms of these ladder operators, we can define the following dimensionless Hamiltonian \mathcal{H}_D

$$\mathcal{H}_D = \begin{bmatrix} 0 & -i\theta^- \\ i\theta^+ & 0 \end{bmatrix}, \quad (22)$$

that acts on the x -dependent pseudo-spinors

$$\Psi_n(x) = \frac{1}{\sqrt{2^{(1-\delta_{0n})}}} \begin{pmatrix} (1 - \delta_{0n}) \psi_{n-1}(x) \\ i \psi_n(x) \end{pmatrix}, \quad n = 0, 1, 2, \dots \quad (23)$$

3 Annihilation operator

In order to build nonlinear coherent states in graphene, one can define a deformed annihilation operator Θ_f given by:

$$\Theta_f^- = \begin{bmatrix} \cos(\delta) \frac{\sqrt{N+2}}{\sqrt{N+1}} f(N+2) \theta^- & \sin(\delta) \frac{f(N+2)}{\sqrt{N+1}} (\theta^-)^2 \\ -\sin(\delta) f(N+1) \sqrt{N+1} & \cos(\delta) f(N+1) \theta^- \end{bmatrix}, \quad \Theta_f^+ = (\Theta_f^-)^\dagger, \quad (24)$$

such that

$$\Theta_f^- \Psi_n(x, y) = \frac{f(n)}{\sqrt{2^{\delta_{1n}}}} \exp(i\delta) \sqrt{n} \Psi_{n-1}(x, y), \quad n = 0, 1, 2, \dots, \quad (25)$$

where $f(N)$ is again a well-behaved function of the number operator $N = \theta^+ \theta^-$. Also, the operators Θ_f^\pm satisfy the nonlinear algebra

$$[\Theta_f^-, \Theta_f^+] = \begin{bmatrix} \Omega(N+1) & 0 \\ 0 & \Omega(N) \end{bmatrix}, \quad \Omega(N) = (N+1)f^2(N+1) - Nf^2(N). \quad (26)$$

In the limit $f(N) = 1$, we have that $[\Theta_f^-, \Theta_f^+] = \mathbb{I}$, where \mathbb{I} is the 2×2 identity matrix, *i.e.*, we recover the HW algebra.

3.1 Nonlinear coherent states

We can construct NLCS $\Psi_\alpha^f(x, y)$ as eigenstates of the operator Θ_f^- :

$$\Theta_f^- \Psi_\alpha^f(x, y) = \alpha \Psi_\alpha^f(x, y), \quad \alpha \in \mathbb{C}, \quad (27)$$

where

$$\Psi_\alpha^f(x, y) = a_0 \Psi_0(x, y) + \sum_{n=1}^{\infty} a_n \Psi_n(x, y). \quad (28)$$

Upon inserting these states into the corresponding eigenvalue equation, we get the following relations:

$$a_1 f(1) = \sqrt{2} \tilde{\alpha} a_0, \quad a_{n+1} f(n+1) \sqrt{n+1} = \tilde{\alpha} a_n. \quad (29)$$

3.1.1 Case for $f(1) \neq 0$

If $f(1) \neq 0$, a_0 turns out to be a free parameter. Thus, the NLCS are

$$\Psi_\alpha^f(x, y) = a_0 \left[\Psi_0(x, y) + \sum_{n=1}^{\infty} \frac{\sqrt{2}\tilde{\alpha}^n}{[f(n)]!\sqrt{n!}} \Psi_n(x, y) \right], \quad (30)$$

where

$$[f(n)]! \equiv \begin{cases} 1 & \text{for } n = 0, \\ f(1) \cdots f(n) & \text{for } n \neq 0. \end{cases} \quad (31)$$

3.1.2 Case for $f(1) = 0$

If $f(1) = 0$, we have that $a_0 = 0$, so that we can consider two new cases, as follows:

a) $f(2) \neq 0$ In this case, a_1 is the new free parameter. Therefore, the NLCS are

$$\Psi_\alpha^f(x, y) = a_1 \sum_{n=0}^{\infty} \frac{\tilde{\alpha}^n}{[g(n)]!\sqrt{(n+1)!}} \Psi_{n+1}(x, y), \quad (32)$$

where $g(n) \equiv f(n+1)$.

b) $f(2) = 0$ Finally, we have that a_2 is the free parameter. The corresponding NLCS are given by

$$\Psi_\alpha^f(x, y) = a_2 \sum_{n=0}^{\infty} \frac{\sqrt{2}\tilde{\alpha}^n}{[h(n)]!\sqrt{(n+2)!}} \Psi_{n+1}(x, y), \quad (33)$$

where $h(n) \equiv f(n+2)$.

3.2 Some examples

In order to describe the effects of strain on the NLCS in graphene, we consider some particular forms for the function $f(N+1)$ in Θ_f^- [24]. Moreover, we will use some physical quantities to analyze such quantum states, as the probability density $\rho_\alpha(x)$, the mean energy $\langle H_D \rangle$ and the Heisenberg uncertainty relation (HUR). To compute the latter, we define the matrix operator \mathbb{S}_q and its square as

$$\mathbb{S}_q = s_q \otimes \mathbb{I}, \quad \mathbb{S}_q^2 = s_q^2 \otimes \mathbb{I}, \quad (34)$$

where

$$s_q = \frac{1}{\sqrt{2}i^q} (\theta^- + (-1)^q \theta^+), \quad (35a)$$

$$s_q^2 = \frac{1}{2} [2N + 1 + (-1)^q ((\theta^-)^2 + (\theta^+)^2)], \quad (35b)$$

and $q = 0, 1$. The variance of the operator \mathbb{S}_q is calculated as follows:

$$\sigma_{S_q} = \sqrt{\langle \mathbb{S}_q^2 \rangle - \langle \mathbb{S}_q \rangle^2}. \quad (36)$$

Thus, when $q = 0$ ($q = 1$), we have that $\sigma_{S_0} = \sigma_\xi$ ($\sigma_{S_1} = \sigma_p$), *i.e.*, the variance of the position ξ (momentum p) operator and the HUR must fulfill:

$$\sigma_\xi \sigma_p = \sigma_{S_0} \sigma_{S_1} \geq \frac{1}{2}. \quad (37)$$

3.2.1 Case for $f(1) \neq 0$

The simplest form for $f(N)$ that satisfies the condition $f(1) \neq 0$ is $f(N+1) = 1$. For this choice, the corresponding NLCS are given by

$$\Psi_\alpha^f(x, y) = \frac{1}{\sqrt{2 \exp(|\tilde{\alpha}|^2) - 1}} \left[\Psi_0(x, y) + \sum_{n=1}^{\infty} \frac{\sqrt{2} \tilde{\alpha}^n}{\sqrt{n!}} \Psi_n(x, y) \right], \quad (38)$$

whose probability density is depicted in Figs. 2 and 3 and has the analytical form:

$$\begin{aligned} \rho_\alpha(x) &= \Psi_\alpha^f(x, y)^\dagger \Psi_\alpha^f(x, y) \\ &= \frac{1}{2 \exp(|\tilde{\alpha}|^2) - 1} \left[\left| \psi_0^2(x) + \sum_{n=1}^{\infty} \frac{\tilde{\alpha}^n}{\sqrt{n!}} \psi_n(x) \right|^2 \right. \\ &\quad \left. + \left| \sum_{n=1}^{\infty} \frac{\tilde{\alpha}^n}{\sqrt{n!}} \psi_{n-1}(x) \right|^2 + 2\Re \left(\sum_{n=1}^{\infty} \frac{\tilde{\alpha}^n}{\sqrt{n!}} \psi_n(x) \psi_0(x) \right) \right]. \end{aligned} \quad (39)$$

Using these NLCS, the mean values of the operators \mathbb{S}_q and \mathbb{S}_q^2 are, respectively (see Fig. 4):

$$\langle \mathbb{S}_q \rangle_\alpha = \frac{\tilde{\alpha} + (-1)^q \tilde{\alpha}^*}{\sqrt{2} i^q (2 \exp(|\tilde{\alpha}|^2) - 1)} \left[\exp(|\tilde{\alpha}|^2) + \sum_{n=1}^{\infty} \frac{|\tilde{\alpha}|^{2n}}{\sqrt{(n-1)!(n+1)!}} \right], \quad (40a)$$

$$\begin{aligned} \langle \mathbb{S}_q^2 \rangle_\alpha &= \frac{1}{2(2 \exp(|\tilde{\alpha}|^2) - 1)} \left[1 + 4|\tilde{\alpha}|^2 \exp(|\tilde{\alpha}|^2) + (-1)^q (\tilde{\alpha}^2 + \tilde{\alpha}^{*2}) \times \right. \\ &\quad \left. \times \left[\exp(|\tilde{\alpha}|^2) + \sum_{n=1}^{\infty} \frac{\sqrt{n+1} |\tilde{\alpha}|^{2n}}{\sqrt{(n-1)!(n+2)!}} \right] \right], \end{aligned} \quad (40b)$$

while the mean energy $\langle H_D \rangle_\alpha^\zeta$ turns out to be (see Fig. 11):

$$\langle H_D \rangle_\alpha^\zeta = \sqrt{ab} \langle H_D \rangle_\alpha, \quad \langle H_D \rangle_\alpha = \frac{2 v_F \hbar \sqrt{\omega}}{2 \exp(|\tilde{\alpha}|^2) - 1} \sum_{n=1}^{\infty} \frac{|\tilde{\alpha}|^{2n}}{n!} \sqrt{n}, \quad (41)$$

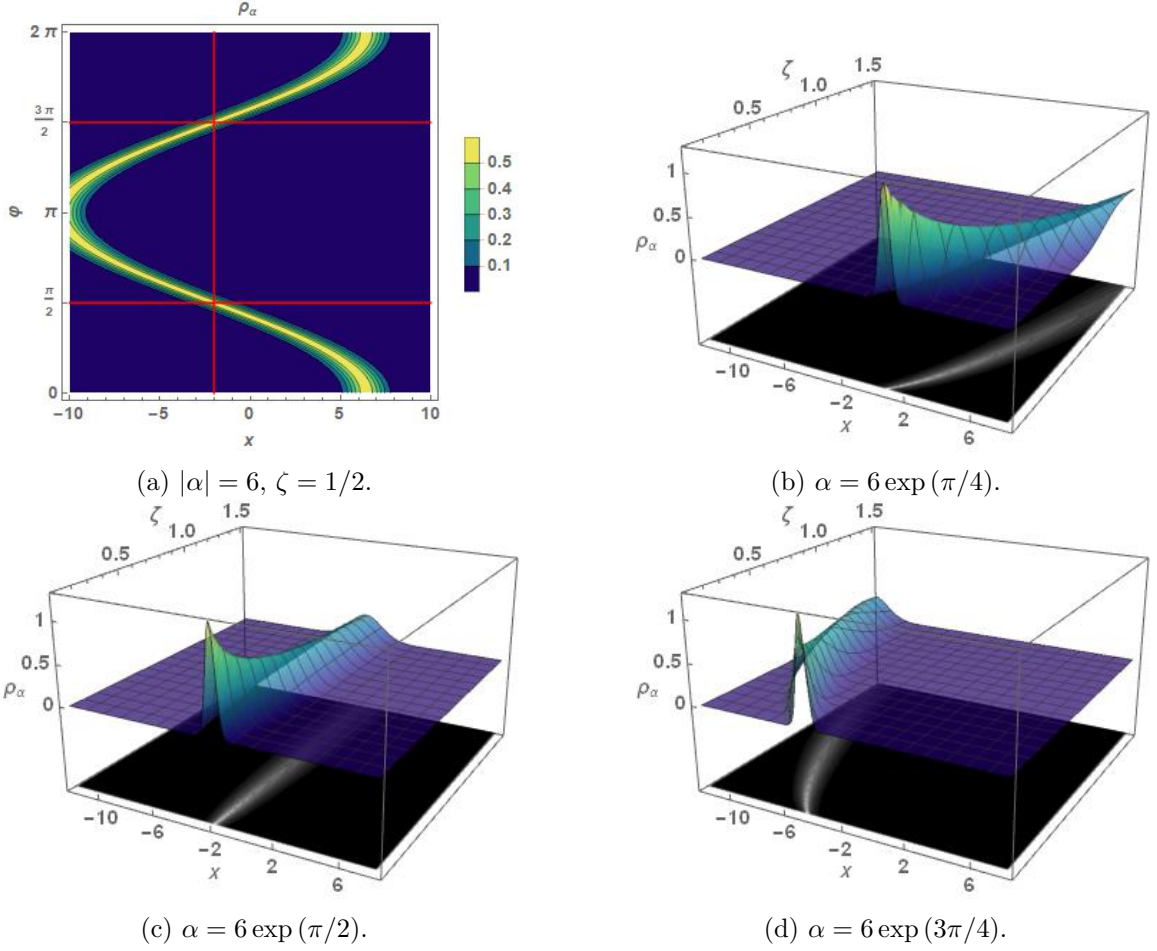


Figure 2: Probability density $\rho_\alpha(x)$ for the coherent states $\Psi_\alpha^f(x, y)$ in Eq. (38) (a) as function of $\varphi = \text{Arg}(\alpha)$ and (b-d) as function of the parameter ζ . In all the cases $B_0 = 1/2$, $k = \omega = 1$ and $\delta = 0$.

where $\langle H_D \rangle_\alpha$ is the mean energy for the pristine graphene for the case $f(1) \neq 0$.

In a semi-classical interpretation, the eigenvalue $\alpha = |\alpha| \exp(i\varphi)$ determines the initial conditions of the motion of the electrons. As $|\alpha|$ changes, the maximum probability density moves along the x -axis, *i.e.*, the center of $\rho_\alpha(x)$ moves away from or approaches to the equilibrium position $x_0 = 2k/\omega$. Also, if $\varphi \in [0, 2\pi]$ varies, the maximum probability performs an oscillatory-like motion around x_0 (vertical red line in Fig. 2a). In particular for $\varphi = \text{Arg}(\alpha) = (2m+1)\pi/2$, $m = 0, 1, \dots$, $\rho_\alpha(x)$ is located around the position x_0 (horizontal red lines in Fig. 2a).

On the other hand, the parameter ζ affects the value of the probability density, as shown in Fig. 2. Similar to what happens with the probability density of the spinorial eigenstates Ψ_n , the function $\rho_\alpha(x)$ grows quickly in the limit $\zeta \rightarrow 0$, while in the opposite regime $\zeta \rightarrow \infty$, $\rho_\alpha(x)$ tends to zero. Moreover, the maximum probability density is located either to the right or to the left of the equilibrium point x_0 according to $0 \leq \varphi < \pi/2$ or $\pi/2 < \varphi \leq 2\pi$. For $\varphi = \pi/2$, the center of $\rho_\alpha(x)$ remains at x_0 .

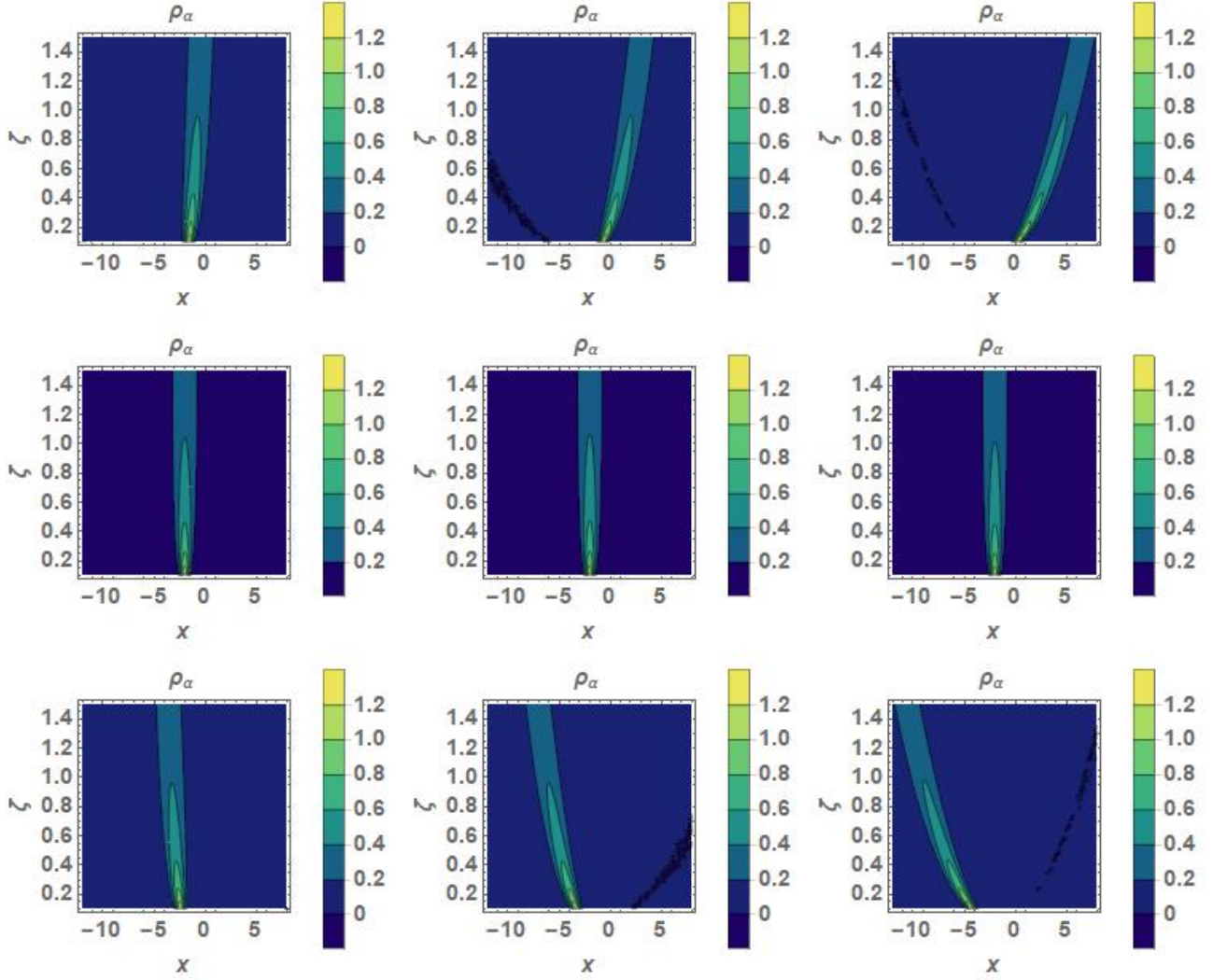


Figure 3: Probability density $\rho_\alpha(x)$ for the coherent states $\Psi_\alpha^f(x, y)$ in Eq. (38) as function of the parameter ζ for different values of eigenvalue $\alpha = |\alpha| \exp(i\varphi)$: (vertical) $|\alpha| = 1, 3, 5$, and (horizontal) $\varphi = \pi/4, \pi/2, 3\pi/4$. In all these cases $B_0 = 1/2$, $k = \omega = 1$ and $\delta = 0$.

Finally, Fig. 4 shows that the Heisenberg uncertainty relation reaches a maximum value for small values of $|\alpha|$ and $\varphi = \pi/4$, while in the limits $\alpha \rightarrow 0$ and $\alpha \rightarrow \infty$ we have that $(\sigma_\xi)_\alpha(\sigma_p)_\alpha \rightarrow 1/2$. This behavior can be understood through the respective variances of the position ξ and momentum p operators: when $\varphi = 0$, the function $\langle S_1 \rangle_\alpha = \langle p \rangle_\alpha = 0$ and the dispersion of the momentum p is smaller than that of the position ξ . As φ grows, the dispersions of each operator change until they are equal ($\varphi = \pi/4$) or their behaviors are exchanged ($\varphi = \pi/2$), *i.e.*, now we have that $\langle S_0 \rangle_\alpha = \langle \xi \rangle_\alpha = 0$. This last circumstance implies that the electron performs symmetric oscillations around the equilibrium position x_0 , in agreement to the previous analysis of the probability density.

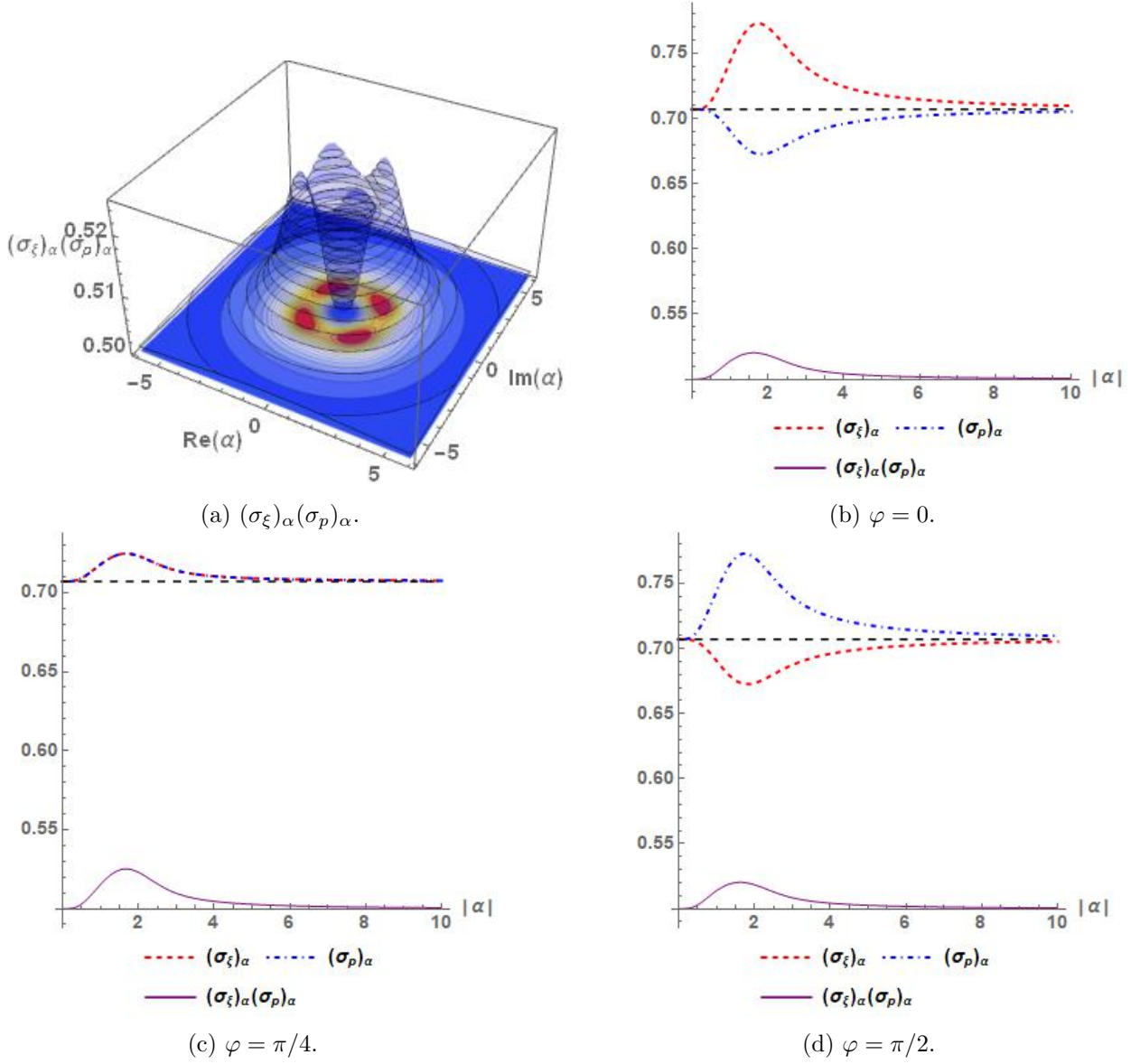


Figure 4: For the states in Eq. (38): (a) $(\sigma_\xi)_\alpha(\sigma_p)_\alpha$ as function of α . (b-d) Comparison between $(\sigma_\xi)_\alpha$, $(\sigma_p)_\alpha$ and $(\sigma_\xi)_\alpha(\sigma_p)_\alpha$ as function of $|\alpha|$. As $|\alpha|$ increases both $(\sigma_\xi)_\alpha$ and $(\sigma_p)_\alpha$ approach the value $1/\sqrt{2}$ and thus their product tends to the value $1/2$. Also, as φ changes, the dispersion of the position ξ is upper, equal or lower than that of the momentum p .

3.2.2 Case for $f(1) = 0$

Now, we consider the case for $f(1) = 0$. As mentioned in the previous section, we can consider two new cases.

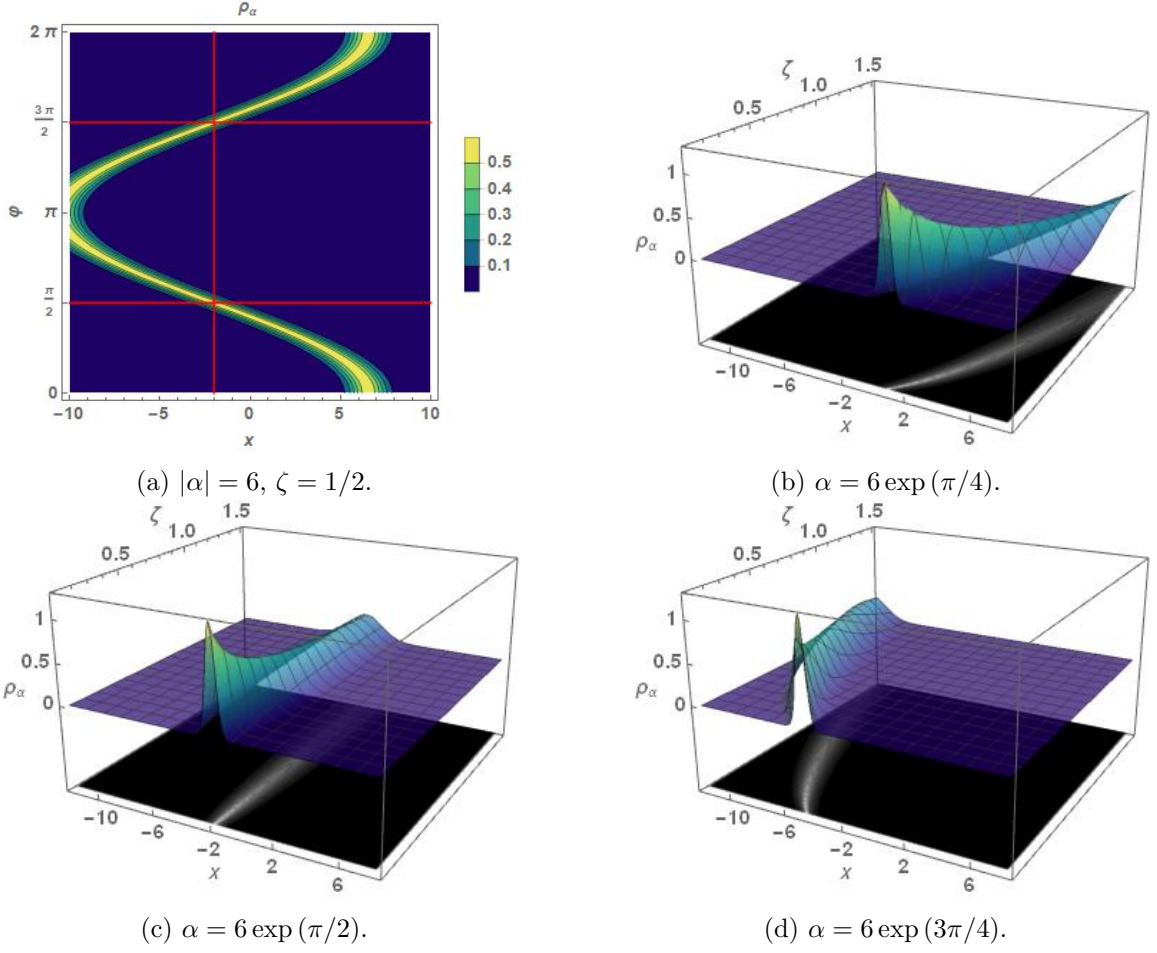


Figure 5: Probability density $\rho_\alpha(x)$ for the coherent states $\Psi_\alpha^f(x, y)$ in Eq. (42) (a) as function of $\varphi = \text{Arg}(\alpha)$ and (b-d) as function of the parameter ζ . In all the cases $B_0 = 1/2$, $k = \omega = 1$ and $\delta = 0$.

a) $f(2) \neq 0$. A function $f(N)$ that satisfy the additional condition $f(2) \neq 0$ is $f(N+1) = g(N) = \sqrt{N}/\sqrt{N+1}$. Hence, the NLCS turn out to be

$$\Psi_\alpha^f(x, y) = \exp\left(-\frac{|\tilde{\alpha}|^2}{2}\right) \sum_{n=0}^{\infty} \frac{\tilde{\alpha}^n}{\sqrt{n!}} \Psi_{n+1}(x, y), \quad (42)$$

and its probability density is (see Figs. 5 and 6):

$$\begin{aligned} \rho_\alpha(x) &= \Psi_\alpha^f(x, y)^\dagger \Psi_\alpha^f(x, y) \\ &= \frac{\exp(-|\tilde{\alpha}|^2)}{2} \left[\left| \sum_{n=0}^{\infty} \frac{\tilde{\alpha}^n}{\sqrt{n!}} \psi_{n+1}(x) \right|^2 + \left| \sum_{n=0}^{\infty} \frac{\tilde{\alpha}^n}{\sqrt{n!}} \psi_n(x) \right|^2 \right]. \end{aligned} \quad (43)$$

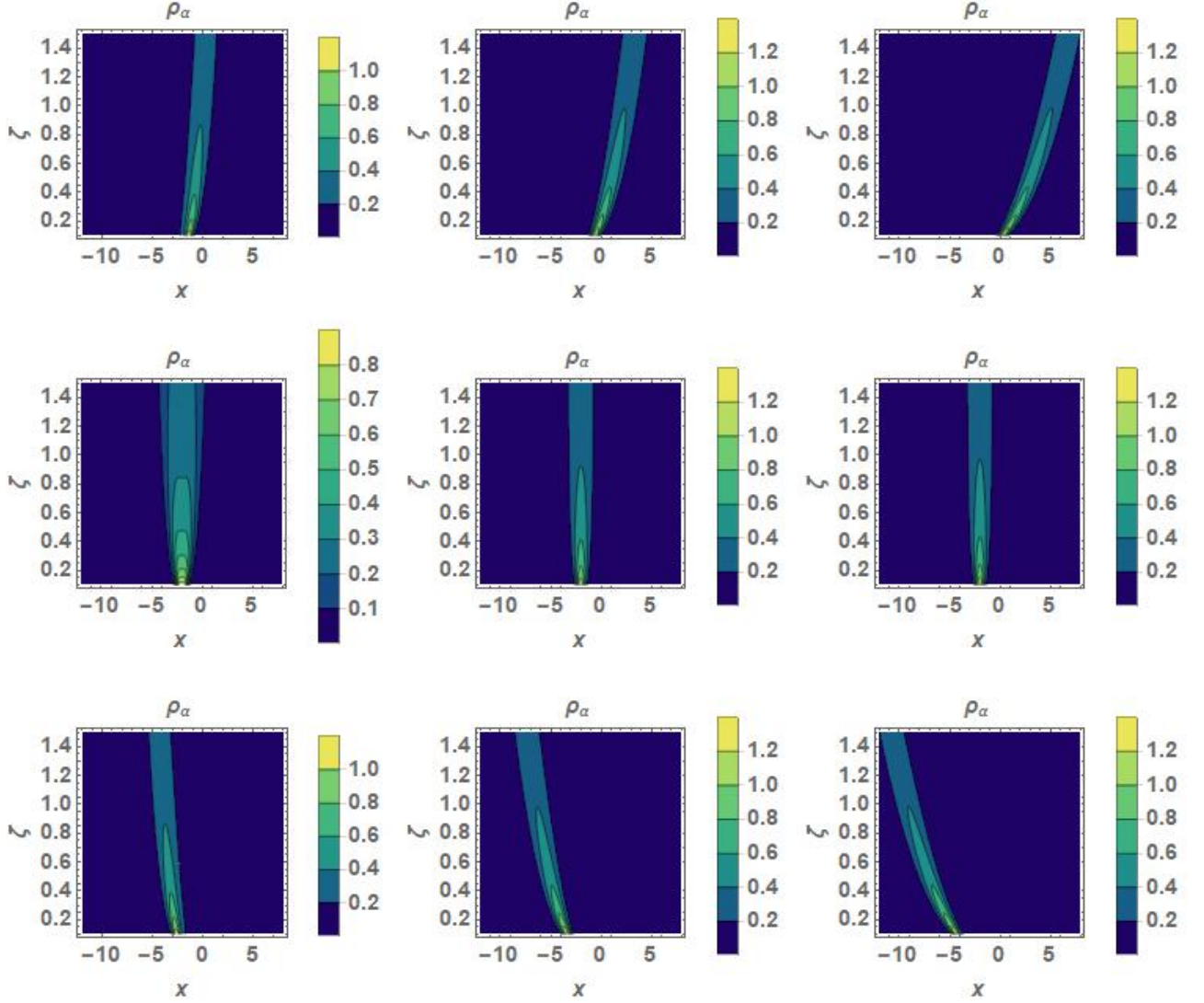


Figure 6: Probability density $\rho_\alpha(x)$ for the coherent states $\Psi_\alpha^f(x, y)$ in Eq. (42) as function of the parameter ζ for different values of eigenvalue $\alpha = |\alpha| \exp(i\varphi)$: (vertical) $|\alpha| = 1, 3, 5$, and (horizontal) $\varphi = \pi/4, \pi/2, 3\pi/4$. In all these cases $B_0 = 1/2$, $k = \omega = 1$ and $\delta = 0$.

The mean values of the operators \mathbb{S}_q and \mathbb{S}_q^2 in this representation are, respectively (see Fig. 7):

$$\langle \mathbb{S}_q \rangle_\alpha = \frac{\tilde{\alpha} + (-1)^q \tilde{\alpha}^*}{2\sqrt{2}i^q} \left[1 + \exp(-|\tilde{\alpha}|^2) \sum_{n=0}^{\infty} \frac{\sqrt{n+2} |\tilde{\alpha}|^{2n}}{\sqrt{n!(n+1)!}} \right], \quad (44a)$$

$$\begin{aligned} \langle \mathbb{S}_q^2 \rangle_\alpha &= 1 + |\tilde{\alpha}|^2 \\ &+ (-1)^q \frac{(\tilde{\alpha}^2 + \tilde{\alpha}^{*2})}{4} \left[1 + \exp(-|\tilde{\alpha}|^2) \sum_{n=0}^{\infty} \frac{\sqrt{n+3} |\tilde{\alpha}|^{2n}}{\sqrt{n!(n+1)!}} \right], \end{aligned} \quad (44b)$$

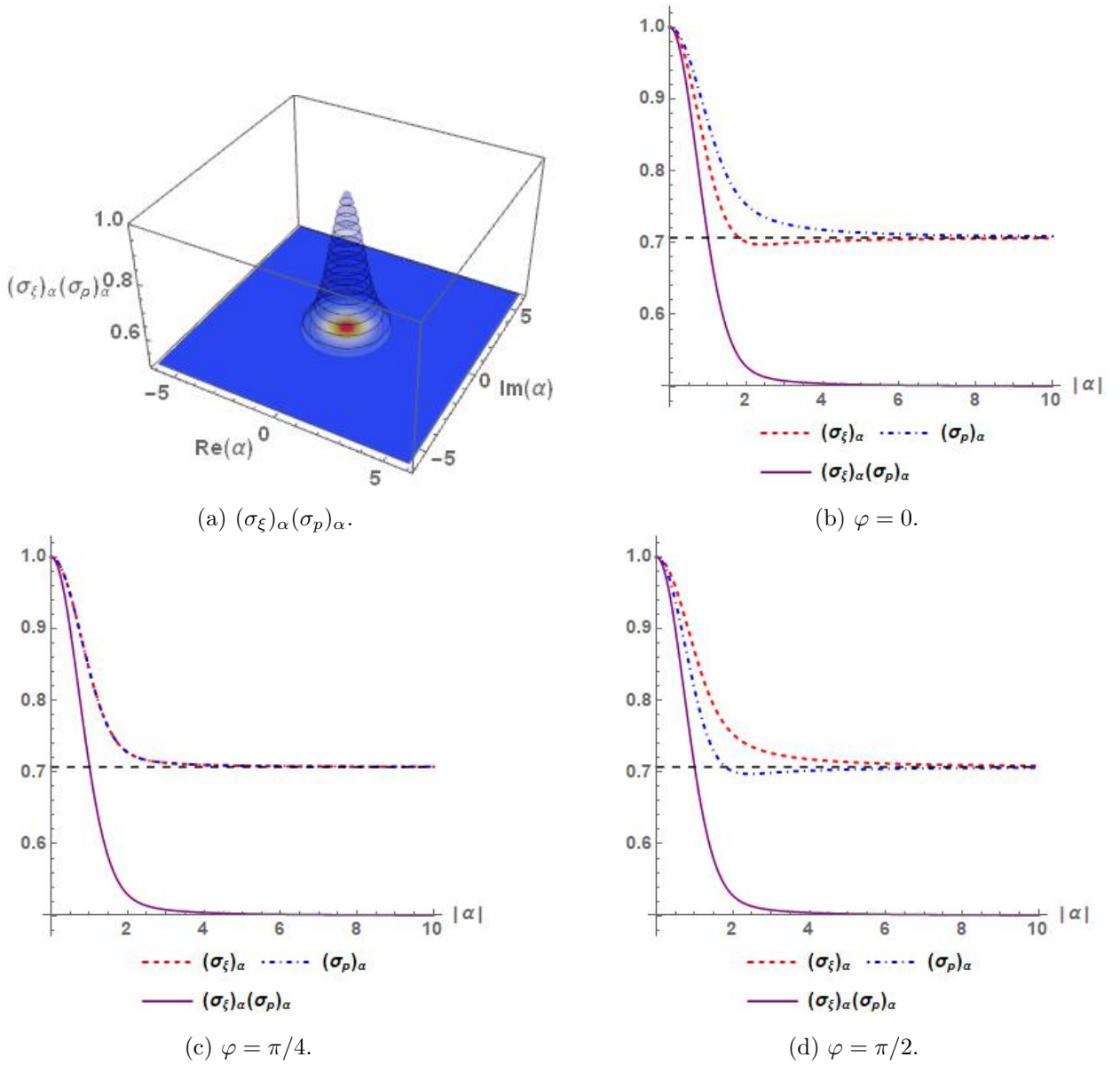


Figure 7: For the states in Eq. (42): (a) $(\sigma_\xi)_\alpha(\sigma_p)_\alpha$ as function of α . (b-d) Comparison between $(\sigma_\xi)_\alpha$, $(\sigma_p)_\alpha$ and $(\sigma_\xi)_\alpha(\sigma_p)_\alpha$ as function of $|\alpha|$. As $|\alpha|$ increases both $(\sigma_\xi)_\alpha$ and $(\sigma_p)_\alpha$ approach the value $1/\sqrt{2}$ and thus their product tends to $1/2$. Also, as φ changes, the dispersion of the position ξ is lower, equal or upper than that of the momentum p .

while the mean energy $\langle H_D \rangle_\alpha^\zeta$ is (see Fig. 11):

$$\langle H_D \rangle_\alpha^\zeta = \sqrt{ab} \langle H_D \rangle_\alpha, \quad \langle H_D \rangle_\alpha = \frac{v_F \hbar \sqrt{\omega}}{\exp(|\tilde{\alpha}|^2)} \sum_{n=0}^{\infty} \frac{|\tilde{\alpha}|^{2n}}{n!} \sqrt{n+1}, \quad (45)$$

where $\langle H_D \rangle_\alpha$ is the corresponding mean energy for the pristine graphene for the same function $g(N)$.

Analogously to the previous case, the center of the corresponding $\rho_\alpha(x)$ moves away from or approaches to the equilibrium position x_0 as $|\alpha|$ increases or decreases, respectively. By varying $\varphi \in [0, 2\pi]$, the maximum probability performs again an oscillatory-like motion around x_0 (vertical red line in Fig. 5a), but when $\varphi = (2m + 1)\pi/2$, $m = 0, 1, \dots$, $\rho_\alpha(x)$ is centered in such position (horizontal red lines in Fig. 5a).

Moreover, the parameter ζ affects the probability density (see Fig. 5): the value of $\rho_\alpha(x)$ increases in the limit $\zeta \rightarrow 0$, while it tends to zero for $\zeta \rightarrow \infty$. Additionally, the center of the probability density is located either to the right, to the left or at the equilibrium point x_0 according to $0 \leq \varphi < \pi/2$, $\pi/2 < \varphi \leq 2\pi$ or $\varphi = \pi/2$, respectively.

On the other hand, Fig. 7 shows that the Heisenberg uncertainty relation reaches a maximum value equal to 1 in the limit $\alpha \rightarrow 0$, while it tends quickly to the minimum uncertainty value when $\alpha \rightarrow \infty$. In contrast to the previous case, this behavior is due to the state $\Psi_1(x, y)$, which is the minimum energy state that contributes to the corresponding superposition $\Psi_\alpha^f(x, y)$ in Eq. (42). Likewise, for values of $|\alpha|$ close to zero and φ growing, the variances of the position ξ and momentum p operators change with respect to each other, becoming equal only when $\varphi = \pi/4$ but always being different to the usual value obtained for the standard coherent states of the harmonic oscillator. In particular, this implies that as $|\alpha|$ increases the uncertainty in the position reduces, as much as the quantum nature of such states allows.

b) $f(2) = 0$. Finally, for this case we consider the function $f(N + 2) = h(N) = \sqrt{N} \times \sqrt{N+1}/\sqrt{N+2}$, which satisfies the condition $f(2) = 0$. The corresponding NLCS are given by

$$\Psi_\alpha^f(x, y) = \left(\frac{|\tilde{\alpha}|}{I_1(2|\tilde{\alpha}|)} \right)^{1/2} \sum_{n=0}^{\infty} \frac{\tilde{\alpha}^n}{\sqrt{n!(n+1)!}} \Psi_{n+2}(x, y), \quad (46)$$

where $I_1(x)$ denotes the Bessel function of first kind. The probability density is then (see Figs. 8 and 9)

$$\begin{aligned} \rho_\alpha(x) &= \Psi_\alpha^f(x, y)^\dagger \Psi_\alpha^f(x, y) \\ &= \left(\frac{|\tilde{\alpha}|}{2 I_1(2|\tilde{\alpha}|)} \right) \left[\left| \sum_{n=0}^{\infty} \frac{\tilde{\alpha}^n}{\sqrt{n!(n+1)!}} \psi_{n+2}(x) \right|^2 + \left| \sum_{n=0}^{\infty} \frac{\tilde{\alpha}^n}{\sqrt{n!(n+1)!}} \psi_{n+1}(x) \right|^2 \right]. \end{aligned} \quad (47)$$

Also, the quantities $\langle \mathbb{S}_q \rangle_\alpha$ and $\langle \mathbb{S}_q^2 \rangle_\alpha$ are (see Fig. 10):

$$\begin{aligned} \langle \mathbb{S}_q \rangle_\alpha &= \frac{\tilde{\alpha} + (-1)^q \tilde{\alpha}^*}{2\sqrt{2}i^q} \left(\frac{|\tilde{\alpha}|}{I_1(2|\tilde{\alpha}|)} \right) \left[\sum_{n=0}^{\infty} \frac{|\tilde{\alpha}|^{2n}}{\sqrt{n![(n+1)!]^3}} \right. \\ &\quad \left. + \sum_{n=0}^{\infty} \frac{\sqrt{n+3} |\tilde{\alpha}|^{2n}}{\sqrt{n!(n+2)!(n+1)!}} \right], \end{aligned} \quad (48a)$$

$$\begin{aligned} \langle \mathbb{S}_q^2 \rangle_\alpha &= 2 + |\tilde{\alpha}| \frac{I_2(2|\tilde{\alpha}|)}{I_1(2|\tilde{\alpha}|)} + (-1)^q \frac{(\tilde{\alpha}^2 + \tilde{\alpha}^{*2})}{4} \left(\frac{|\tilde{\alpha}|}{I_1(2|\tilde{\alpha}|)} \right) \times \\ &\quad \times \left[\sum_{n=0}^{\infty} \frac{|\tilde{\alpha}|^{2n}}{\sqrt{n!(n+2)!(n+1)!}} + \sum_{n=0}^{\infty} \frac{\sqrt{n+4} |\tilde{\alpha}|^{2n}}{\sqrt{n!(n+1)!(n+2)!}} \right], \end{aligned} \quad (48b)$$

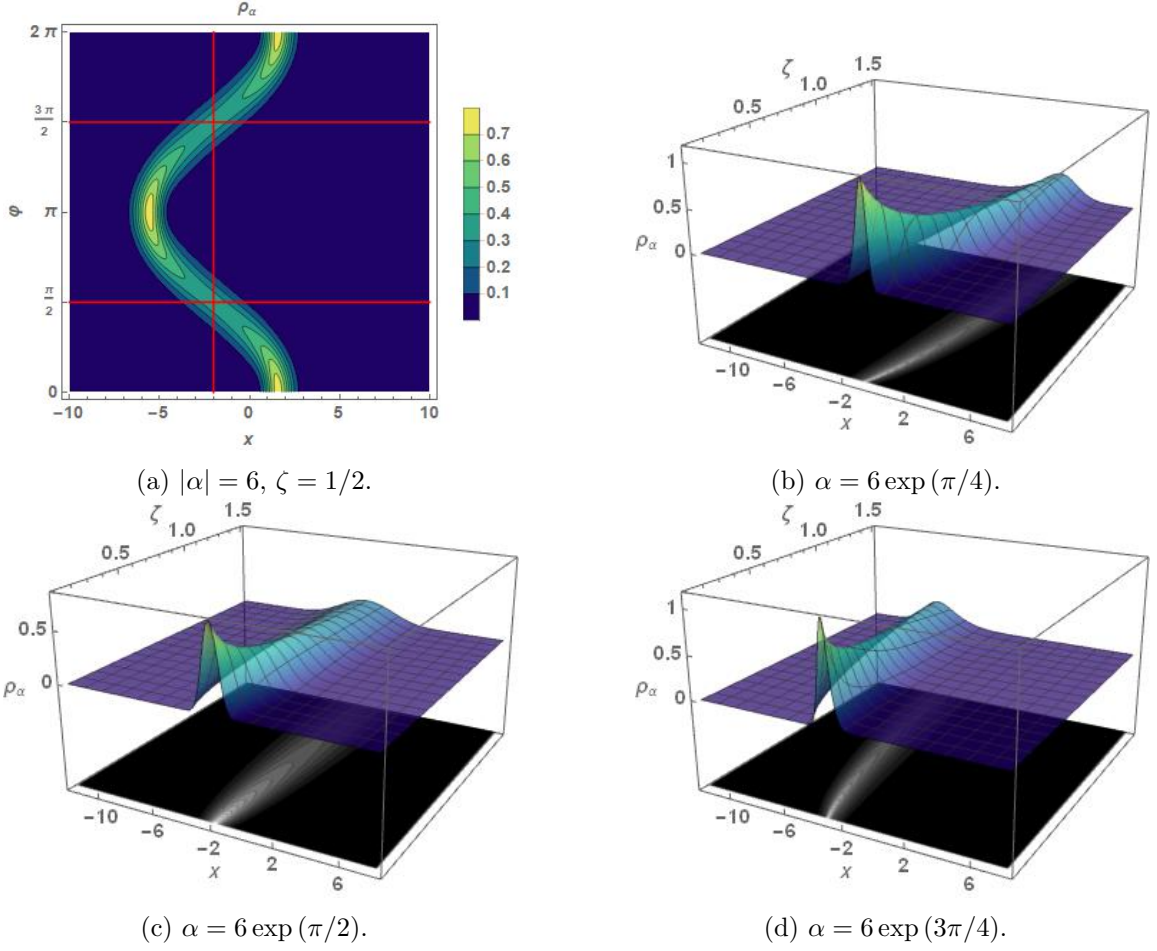


Figure 8: Probability density $\rho_\alpha(x)$ for the coherent states $\Psi_\alpha^f(x, y)$ in Eq. (46) (a) as function of $\varphi = \text{Arg}(\alpha)$ and (b-d) as function of the parameter ζ . In all these cases $B_0 = 1/2$, $k = \omega = 1$ and $\delta = 0$.

and the mean energy $\langle H_D \rangle_\alpha^\zeta$ is given by (see Fig. 11):

$$\langle H_D \rangle_\alpha^\zeta = \sqrt{ab} \langle H_D \rangle_\alpha, \quad \langle H_D \rangle_\alpha = \frac{v_F \hbar \sqrt{\omega} |\tilde{\alpha}|}{I_1(2|\tilde{\alpha}|)} \sum_{n=0}^{\infty} \frac{|\tilde{\alpha}|^{2n}}{n!(n+1)!} \sqrt{n+2}, \quad (49)$$

where $\langle H_D \rangle_\alpha$ is the corresponding mean energy for the pristine graphene for the function $h(N)$.

Once again, the parameter ζ affects the probability density $\rho_\alpha(x)$ in Eq. (47) in a similar manner to the previous cases, changing also the center of such function with respect to the equilibrium position according to the value of $\varphi \in [0, 2\pi]$ (see Fig. 8). However, while the position x of the center of the probability density $\rho_\alpha(x)$ along the x -axis also changes with respect to x_0 due to the values of $\alpha = |\alpha| \exp(i\varphi)$ (vertical and horizontal red lines in Fig. 8a), the distance between the points x and x_0 is smaller in comparison with the cases already discussed.

Furthermore, Fig. 10 shows that the behavior of the Heisenberg uncertainty relation asso-

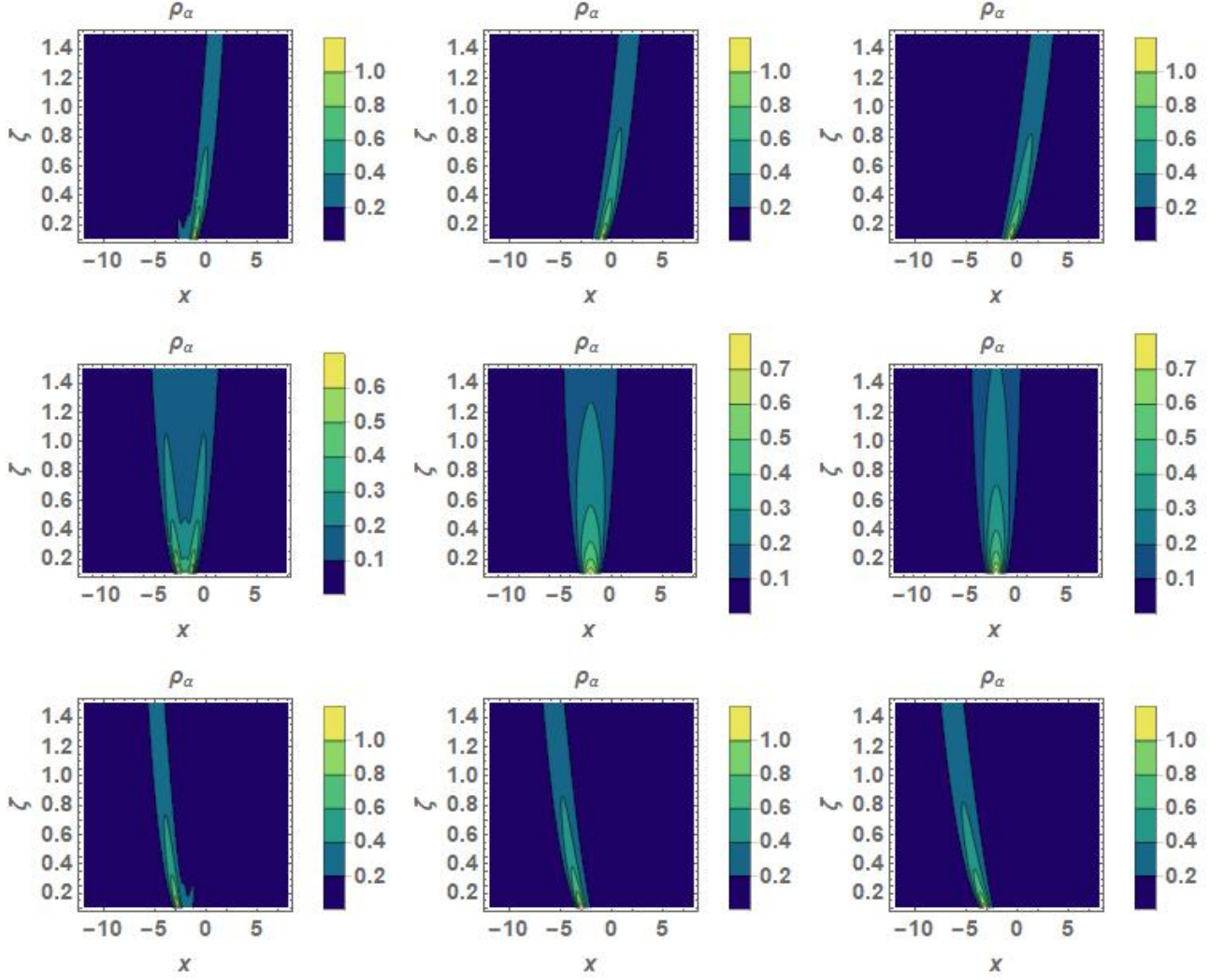


Figure 9: Probability density $\rho_\alpha(x)$ for the coherent states $\Psi_\alpha^f(x, y)$ in Eq. (46) as function of the parameter ζ for different values of eigenvalue $\alpha = |\alpha| \exp(i\varphi)$: (vertical) $|\alpha| = 1, 3, 5$, and (horizontal) $\varphi = \pi/4, \pi/2, 3\pi/4$. In all these cases $B_0 = 1/2$, $k = \omega = 1$ and $\delta = 0$.

ciated to the states in Eq. (46) and variances of the position ξ and momentum p operators are different compared with the previous cases. Now, the HUR reaches a maximum value equal to 2 in the limit $\alpha \rightarrow 0$ but for $\alpha \rightarrow \infty$ it tends very slowly to $1/2$. This behavior is because the state $\Psi_2(x, y)$ is the minimum energy state that appears in the linear combination of $\Psi_\alpha^f(x, y)$ and so these NLCS cannot be considered as minimum uncertainty states. However, the behavior of the variances of both ξ and p operators in the limit $|\alpha| \rightarrow \infty$, suggest a squeezed-like behavior for them.

Finally, Fig. 11 shows a comparison between the mean energy $\langle H_D \rangle_\alpha^\zeta$ corresponding to each NLCS $\Psi_\alpha^f(x, y)$ above described. As we can see, each mean energy is a continuous function of the eigenvalue α and in the limit, $\alpha \rightarrow 0$ their behaviors are different due to the minimum

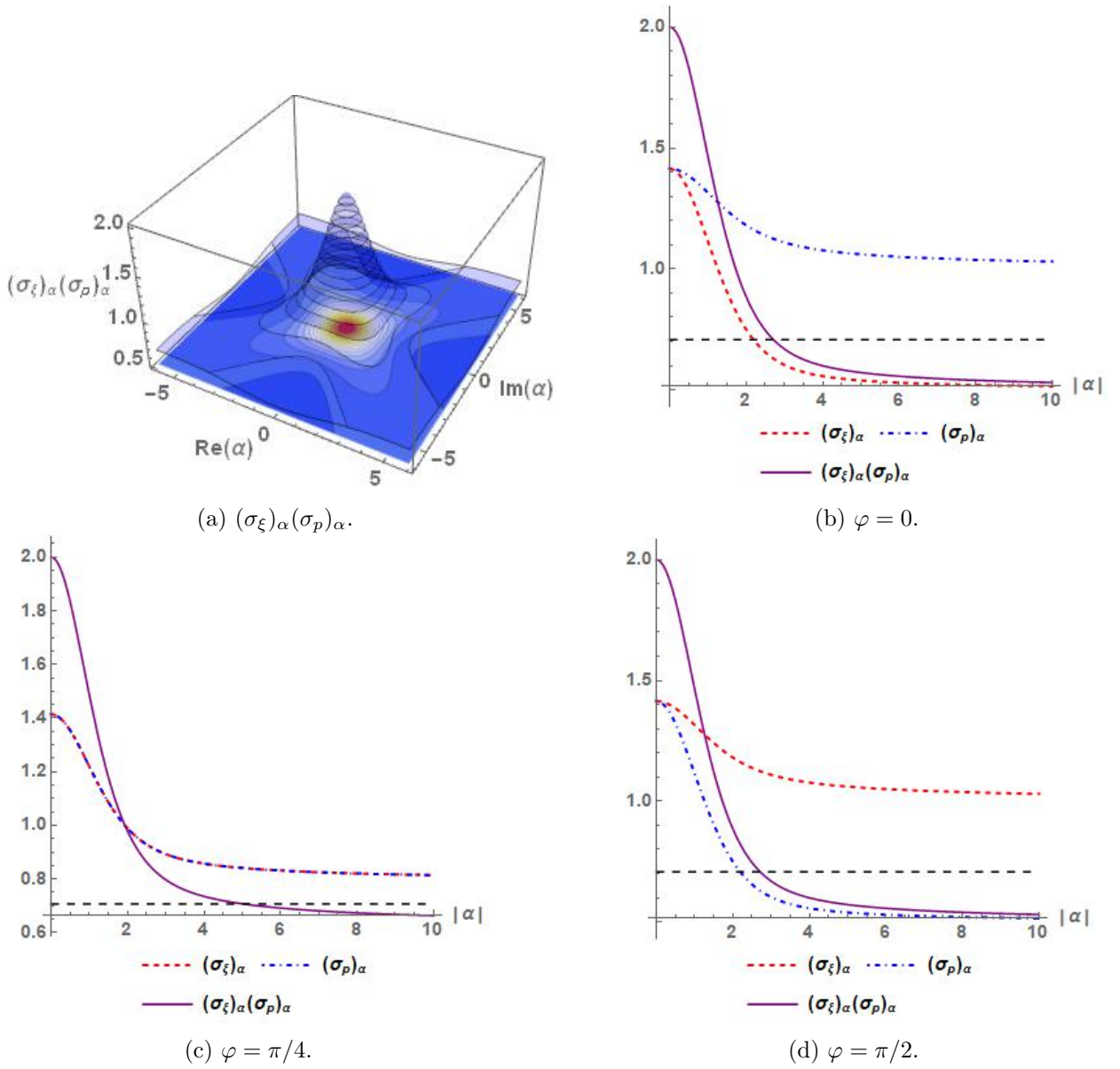


Figure 10: For the states in Eq. (46): (a) $(\sigma_\xi)_\alpha(\sigma_p)_\alpha$ as function of α . (b-d) Comparison between $(\sigma_\xi)_\alpha$, $(\sigma_p)_\alpha$ and $(\sigma_\xi)_\alpha(\sigma_p)_\alpha$ as function of $|\alpha|$. Also, as φ changes, the dispersion of the position ξ is lower, equal or upper than that of the momentum p .

energy state $\Psi_n(x)$ that contributes to the respective NLCS. Moreover, the mean energy is affected by the values of the real parameters a and b that characterize the strain.

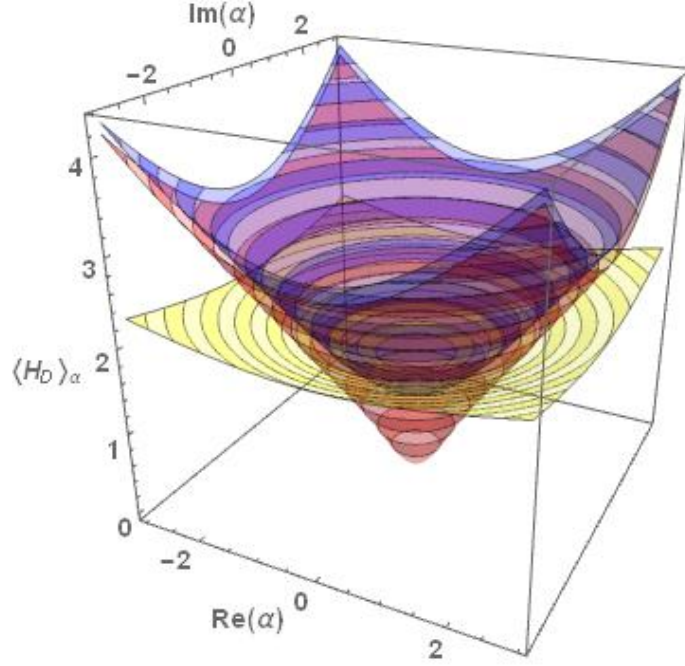


Figure 11: Mean energy $\langle H_D \rangle_\alpha^\zeta / v_F \hbar \sqrt{ab}$ as function of α for the nonlinear coherent states Ψ_α^f : Eq. (41) (red), (45) (blue) and (49) (yellow). In all these cases $B_0 = 1/2$ and $\omega = 1$.

4 Discussion and conclusions

In this work, we have considered a uniform and uniaxially strained graphene layer immersed in a perpendicular uniform magnetic field, in order to explore the effects that the mechanical deformations have in the behavior of the nonlinear coherent states, which can be obtained by describing the background field in a Landau-like gauge. This setup supplies a semi-classical description of the effects that the strain have on the dynamics of the graphene Dirac particles in a magnetic field. For our purposes, the strain is characterized by two dimensionless positive real parameters a and b that, through the quantity $\zeta = a/b$, indicate the direction in which the deformation is applied.

If $0 < \zeta < 1$, the deformation takes place along the y -direction. As a consequence, the probability density of the NLCS is smaller in comparison with the opposite case, $\zeta > 1$, in which the strain is applied along the x -direction. It means that when the graphene layer is deformed along the y -axis, the electrons are confined to move in such direction and the probability to find them in a small interval in the x -axis increases, while if the material is deformed in the orthogonal direction, the region where the electrons can be found increases and the probability decreases as ζ grows.

On the other hand, from a semi-classical point of view, the eigenvalue $\alpha = |\alpha| \exp(i\varphi)$ somehow establishes an initial condition for the coherent states: for $|\alpha|$ -values close to zero, the maximum probability is found around the point x_0 and the effect of the strain is milder than when $|\alpha|$ is larger, allowing to localize the maximum probability away from the point x_0 . In addition, if the center of $\rho_\alpha(x)$ is located to the left ($\varphi > \pi/2$) or to the right ($\varphi < \pi/2$)

of the point x_0 , when a deformation is applied along the x -axis, the distance between those points increases in the respective direction. It is important to remark that the CS obtained for the case $f(1) = f(2) = 0$ tend to stay localized around the point x_0 even if the strain in the x -direction grows.

For experimental considerations, we believe that the results obtained in this article can be useful to explore quantum electronics with graphene through the Wigner function associated to the NLCS. Moreover, an alternative description of our finding can be obtained assuming a symmetric gauge for the background field, in order to describe either the bidimensional effects of the uniform and uniaxial strain on a graphene layer lying on the xy -plane or by considering the problem where the parameters a and b depend on the spatial coordinates. These studies are in progress and will be reported elsewhere.

Acknowledgments

The authors acknowledge David J. Fernández for valuable discussions and careful reading of the manuscript. YCS acknowledges support from CIC-UMSNH under grant 3820801. AR acknowledges support from Consejo Nacional de Ciencia y Tecnología (México) under grant 256494. EDB acknowledges IFM-UMSNH for its warm hospitality and Act. J. Manuel Zapata L. for giving the necessary impulse to continue researching.

References

- [1] V Fock, Z. Phys. **47** (1928) 446
- [2] L Landau, Z. Phys. **64** (1930) 629
- [3] E Schrödinger, Naturwissenschaften **14** (1926) 664-666
- [4] AO Barut, L Girardello, Commun. Math. Phys. **21** (1971) 41-55
- [5] AM Perelomov, Commun. Math. Phys. **26** (1972) 222-236
- [6] A Perelomov, *Generalized coherent states and their applications*, Springer, Berlin 1986
- [7] R Gilmore, Ann. Phys. **74** (1972) 391-463
- [8] R Gilmore, Rev. Mex. Fis. **23** (1974) 143-187
- [9] VI Man'ko, G Marmo, F Zaccaria, ECG Sudarshan, in: Atakishiyev, N., Seligman, T.H. (Eds.) *Proceedings of the IV Wigner Symposium*, World Scientific, New York, 1996, pp. 421
- [10] VI Man'ko, G Marmo, ECG Sudarshan, F Zaccaria, Phys. Scripta **55** (1997) 528
- [11] RL de Matos Filho, W Vogel, Phys. Rev. A **54** (1996) 4560

- [12] S Sivakumar, J. Opt. B: Quantum Semiclass. Opt. **2** (2000) R61
- [13] D Bonatsos, C Daskaloyannis, Phys. Rev. A **46** (1992) 75
- [14] D Bonatsos, C Daskaloyannis, Phys. Rev. A **48** (1993) 3611
- [15] KS Novoselov, E McCann, SV Morozov, VI Falko, MI Katsnelson, U Zeitler, D Jiang, F Schedin, AK Geim, Nat. Phys. **2** (2006) 177 <http://dx.doi.org/10.1038/nphys245>
- [16] MI Katsnelson, Mater. Today **10** (2007) 20
- [17] KS Novoselov, Z Jiang, Y Zhang, SV Morozov, HL Stormer, U Zeitler, JC Maan, GS Boebinger, P Kim, AK Geim, Science **315** (2007) 1379
- [18] AK Geim, KS Novoselov, Nat. Mater. **6** (2007) 183
- [19] VM Pereira, AH Castro Neto, NMR Peres, Phys. Rev. B **80** (2009) 045401
- [20] G García-Naumis, S Barraza-Lopez, M Oliva-Leyva, H Terrones, Rep. Prog. Phys. **80** (2017) 096501
- [21] T Tsoukleri, J Parthenios, K Papagelis, R Jalil, AC Ferrari, AK Geim, KS Novoselov, C Galiotis, Small **5** (2009) 2397
- [22] M Oliva-Leyva, G García-Naumis, Phys. Rev. B **88** (2013) 085430
- [23] Y Betancur-Ocampo, ME Cifuentes-Quintal, G Cordourier-Maruri, R de Coss, Ann. Phys. **359** (2015) 243
- [24] E Díaz-Bautista, DJ Fernández, Eur Phys. J. Plus **132** (2017) 499